

Surface nuclear magnetic relaxation and dynamics of water and oil in macroporous media

S. Godefroy,^{1,2} J.-P. Korb,^{1,*} M. Fleury,² and R. G. Bryant³

¹*Laboratoire de Physique de la Matière Condensée, UMR 7643 CNRS, École Polytechnique, 91128 Palaiseau, France*

²*Institut Français du Pétrole, 92852 Rueil-Malmaison, France*

³*Department of Chemistry, University of Virginia, Charlottesville, Virginia 22901*

(Received 25 September 2000; revised manuscript received 14 May 2001; published 24 July 2001)

Proton nuclear spin-relaxation studies on water- or oil-saturated granular packings and limestone rocks allow estimating surface molecular dynamical parameters. Measurements were performed at various conditions of temperature, magnetic field strengths, and pore size. We show by low field NMR relaxation that changing the amount of surface paramagnetic impurities leads to striking different pore-size dependences of the relaxation times T_1 and T_2 of liquids in pores. These dependences are well supported by surface-limited or diffusion-limited relaxation models. Surface relaxivity parameters ρ_1 and ρ_2 are deduced from the pore-size dependence in the surface-limited regime. We evidence the frequency and temperature dependence of the surface relaxivity ρ_1 by field cycling NMR relaxation and relevant theoretical models. The typical frequency dependence found allows an experimental separation of the surface and bulk microdynamics in porous media. Several surface dynamical parameters, such as diffusion coefficients, activation energies, time of residence, and coefficient of surface affinity, were therefore determined. The methods presented here give a powerful analysis of the surface microdynamics of confined liquids, which can be applied to the study of oil-bearing rocks.

DOI: 10.1103/PhysRevE.64.021605

PACS number(s): 45.70.-n, 76.60.-k, 68.08.-p

I. INTRODUCTION

How is it possible to obtain structure and dynamic information on liquids at pore surface by nuclear spin-relaxation methods? The question is central to understanding texture and transport properties in high surface-area microporous materials, chromatographic supports, heterogeneous catalytic materials, and cement and natural macroporous materials, such as clays, minerals, or porous rocks. However, probing directly the molecular surface dynamics by standard nuclear relaxation methods is difficult. For instance, the very low fraction of molecules in a surface layer in fast exchange with the local bulk phase prevents any direct measurement of the surface molecular dynamics. Several attempts have been proposed to probe surface molecular behavior by standard techniques [1–6]. For example, a progressive saturation of cement has permitted the isolation of the surface contribution to spin-spin relaxation rates [2]. This method, difficult to realize in practice, has permitted a check of the validity of the biphasic fast exchange model in porous media by the linear dependence of relaxation rates with the saturation factor [1]. The spin-spin and spin-lattice relaxation rate measurements for a series of saturated calibrated microporous silica glasses, with or without surface silanization, has allowed separation of the surface and bulk contributions [3–5], thus leading to information on the surface reorientational dynamics [6]. Nonstandard nuclear magnetic relaxation dispersion experiments (NMRD) [7] were also proposed [8–11]. For instance, these methods have shown striking differences between water and aprotic liquids in contact with microporous glass surfaces containing trace paramagnetic impurities [10,11]. All these experimental attempts were con-

cerned so far with high surface-area materials. Here we propose to extend their domain of application to macroporous systems with a low surface to volume ratio, such as oil-bearing rocks. Previous work in the field was concerned with fixed low field NMR relaxation, both in laboratory measurements and in well logging applications [12–16]. This approach allows the estimation of fundamental petrophysical properties, such as porosity, permeability, saturation, pore size distribution, and surface wettability [12–16].

Our aim here is precisely to characterize fundamental surface dynamical properties, such as water and oil surface correlation times, surface diffusion coefficients, surface residence times, and coefficients of surface molecular affinity. Moreover, to obtain these parameters from a nuclear spin-relaxation study, some questions exist concerning the characterization of the nuclear spin processes at the pore surface. These processes depend mainly on the nature of the liquid and on its affinity for the pore surface.

In the present study, we answer these questions by using both nuclear relaxation at 2.2 MHz and field cycling NMRD techniques applied to different kinds of water- or oil-saturated macroporous media. One kind of sample consists of packing of calibrated SiC grains, with 25% of the surface covered by SiO₂, leading to a series of porous media varying in pore sizes in the range of those of oil-bearing rocks. The other kind of sample consists of fine-grain limestone rock cores. Both kinds of samples are homogeneous in pore size. We evidence the presence of Fe³⁺ and Mn²⁺ paramagnetic ions by electron spin resonance (ESR) for grain packing and limestone, respectively. We show by nuclear relaxation measurements at 2.2 MHz that changing the amount of surface paramagnetic impurities, by hydrochloric acid cleaning, leads to striking different pore size dependences of spin-lattice and spin-spin relaxation times (T_1 and T_2). These ob-

*Author to whom correspondence should be sent. FAX: 33 1 69 33 30 04. Email address: jean-pierre.korb@polytechnique.fr

TABLE I. Sample characteristics.

Grain size (μm)	Pore size ^a (μm)	Specific surface (m^2/g)	Porosity (%)	Permeability (darcy)
150	138	0.026	43.9	15.5
110	100	0.035	42.9	8.4
80	74	0.047	43.8	3.0
50	48	0.078	46.4	1.4
30	27	0.13	44.8	0.4
15	14	0.25	43.4	0.15
8	8.3	0.56	52.6	0.05

^aThese numbers come from grain sizes and the use of Eq. (1).

servations and an analytical model show that the leading relaxation process is either surface limited or diffusion limited. For the surface-limited process, we deduce the surface relaxivity parameters ρ_1 and ρ_2 directly from the pore size dependence of T_1 and T_2 . We report, by the nuclear magnetic relaxation dispersion technique (field cycling NMRD), the frequency and temperature dependence of the surface relaxivity, $\rho_1(\omega_p T)$. We applied this technique to the “cleaned” 8 μm SiC samples and to the Lavoux limestone, saturated either with water or oil. This technique and the theoretical model that we propose permit the separation of the surface liquid microdynamics from the bulk dynamics. We thus estimate surface dynamical parameters as correlation times, surface diffusion coefficients, and surface residence times. We evidence the differences in water and oil surface affinity and deduce a coefficient of surface affinity. Anomalous temperature dependence of relaxation times for the silica surface is also discussed.

II. SAMPLE CHARACTERIZATION

A. Granular porous media

We used model granular porous media made by packing down calibrated silica carbide grains (SiC) from P. Wolters Company (Germany) [17]. The grains were obtained by grinding and were selected in calibrated size by sedimentation in air. The mean grain sizes range individually between 8 and 150 μm , with an accuracy of $\pm 5\%$, with a grain density of 3.2. The grain-specific surface areas measured by nitrogen adsorption-desorption range between 0.56 and 0.026 m^2/g for grain sizes between 8 and 150 μm , respectively (Table I). Individual grains are composed of SiC crystals of size about 0.1 μm cemented by an amorphous SiC phase. X-ray photoelectron spectroscopy (XPS) experiments showed that 25% of the surface is covered by SiO_2 [17], formed by passive oxidation of amorphous silica either for months at room temperature or during a few hours at 350 $^\circ\text{C}$.

This material is convenient to produce model granular porous media [18] obtained by packing down dry calibrated grains in cells of 3 cm in diameter and 5 or 10 cm in length. The cells are composed of a glass tube and two caps allowing fluid circulation, and bearing pressure up to 5 bars to avoid gas formation at high temperature. The porosities ϕ of the various prepared grain packs were obtained both by

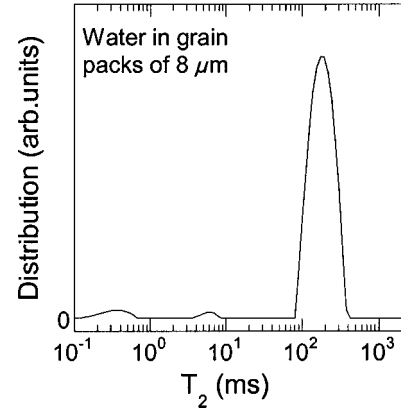


FIG. 1. Example of the ^1H spin-spin relaxation time distribution obtained with the cleaned 8 μm grain pack saturated with water at 2.2 MHz and 34 $^\circ\text{C}$. The intense and narrow peak at 180 ms shows the monodispersity of the pore size distribution. The same measurement has been made for each sample.

NMR and gravimetric methods and are reported in Table I. The almost constant value of the porosity (about 45%) for the various packings show that the main textural properties are preserved although the grain sizes vary. The grains are nonporous by themselves. The resulting pore d_{pore} and grain d_{grain} diameters are related, considering the correspondence between pore volume and solid volume,

$$d_{\text{pore}} = \left(\frac{\phi}{1 - \phi} \right)^{1/3} d_{\text{grain}}. \quad (1)$$

The monodispersity of the pore sizes is evidenced in Fig. 1 by the narrow NMR spin-spin relaxation time (T_2) distribution of water in grain packings of 8 μm . This distribution is obtained by a numerical Laplace inversion of the observed magnetization decay [16]. The inversion involves a regularization method that smooths and broadens the distribution. However, as we used grain packings with narrow pore size distributions, these problems of data inversion are limited. Therefore, in the paper, we use the T_2 value obtained by a monoexponential fit of the relaxation signal corresponding to the geometric mean of the T_2 distribution (peak value), in accordance with the accuracy of the measurement. We have obtained similar distributions for the other grain sizes. The quadratic relation, $K \propto d_{\text{pore}}^{2.0}$, that we observed between the permeability K and the pore size (Fig. 2) is consistent with the Kozeny-Carman relation typically observed in quasi-spherical grain packings. Moreover, this figure gives us confidence about the reproducibility of the texture of the different packings [18,19].

The porous media were saturated either with water or oil (dodecane) in the cells initially under a vacuum of 2×10^{-2} mbar. For water saturation, cycles of vacuum and CO_2 flooding were made to totally remove oxygen in pores. The pore surface contains paramagnetic impurities that originate either from the grinding of the grains or substituted to silica during the production of the SiC material. It is necessary to remove the paramagnetic impurities coming from grinding to perform reliable surface relaxation experiments.

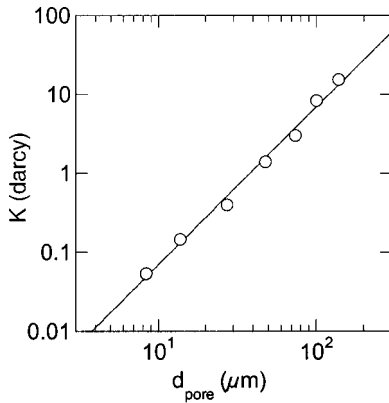


FIG. 2. Variation of the water permeability (K) as a function of the pore diameter (d_{pore}). K is measured for each sample of a set of SiC cleaned calibrated grain packs. The curve fit shows the expected power law $K \propto d_{\text{pore}}^2$.

We thus applied a continuous flux of hydrochloric acid solution in each porous media at a low flow rate, for a few weeks, to clean the surfaces. The acidic solution at the outlet of the grain pack was gathered by a fraction collector every 90 min. Each fraction was analyzed by its spin-spin nuclear relaxation rates $1/T_2$, proportional to the paramagnetic impurity concentration in solution [20]. Figure 3 shows an example of the variation of $1/T_2$ as a function of the cleaning duration as a control of the efficiency of our cleaning procedure. The sharp decrease at short times exhibits the removal of major impurities and iron filings. At longer times, $1/T_2$ tends to an asymptotic value given by the relaxation rate of the pure acidic solution. Of course, this cleaning procedure does not remove paramagnetic impurities chemically substituted to silicon.

The remaining paramagnetic impurities were monitored by electron spin resonance (ESR) for each sample. The experiments were performed on an X-band ESR Bruker spectrometer at room temperature. For instance, Fig. 4 shows the spectra measured for the $80 \mu\text{m}$ grains. The sharp peak at $g=2$ is the signature of free electrons. The extended peak at

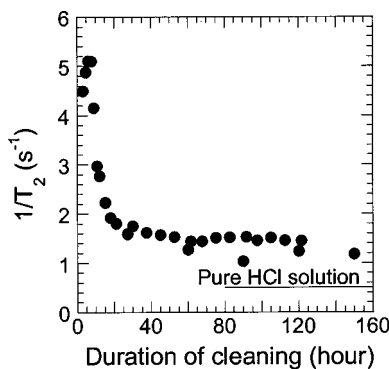


FIG. 3. The ^1H spin-spin relaxation rates ($1/T_2$) of the acidic solution at 2.2 MHz and 34°C , collected at the outlet of the $50 \mu\text{m}$ grain pack as a function of duration of cleaning. At short time, the sharp decrease of $1/T_2$ exhibits the efficiency of the cleaning process. At long time $1/T_2$ tends progressively towards the asymptotic $1/T_2$ of the pure HCl solution represented in the figure.

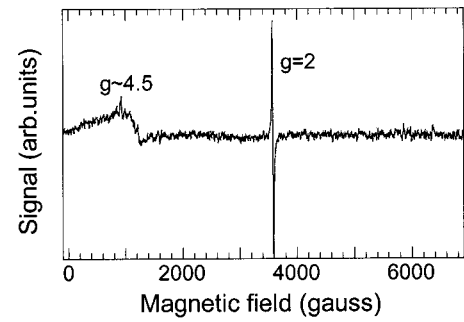


FIG. 4. Electron spin resonance (ESR) spectrum measured at room temperature on the dry grains of diameter $80 \mu\text{m}$. The sharp peak at $g=2$ corresponds to free electrons and the large peak at $g \sim 4.5$ corresponds to the ferric ions Fe^{3+} . The corresponding intensity of Fe^{3+} , obtained by the integration of the peak, is much larger than that of free electrons.

$g \sim 4.5$ represents ferric ion (Fe^{3+}) impurities. The integration of this peak, proportional to the amount of Fe^{3+} , is much larger than that of the peak of electrons. We will see below that ferric ions thus influence the liquid proton relaxation, appending exclusively at the pore surface. The measurement was calibrated by adding a very small crystal of CuSO_4 of known weight in the sample. This allows an estimation of the quantity of paramagnetic impurities per gram of material. We measured the same number of Fe^{3+} ions per gram over the whole set of cleaned grain sizes after correcting the data only for the large grain sizes due to the skin effect. This confirms the homogeneous volume repartition of the paramagnetic ferric ions. We thus deduce the proportion of surface impurities, to which relaxation of fluid protons of the saturated porous media will be sensitive, by $S_p \rho_d \delta$, where S_p is the specific surface area, ρ_d the grain density, and $\delta = 3.6 \text{ \AA}$ is the silicon interatomic distance [10]. The proportion of the surface compared to the total amount of impurities is thus about 0.065% for the $8 \mu\text{m}$ grains and the surface density of impurities is $\sigma_s = 1.7 \times 10^{13} \text{ Fe}^{3+}/\text{cm}^2$.

B. Limestone

We used cores of fine grain Lavoux limestone of diameters and lengths 4 and 3 cm and 0.8 and 1.5 cm, respectively. The cores were water- or oil- (dodecane) saturated under vacuum. The narrow pore size distribution was evidenced by the narrow transverse relaxation time distribution of the water-saturated core (Fig. 5). Paramagnetic impurities species of the limestone were analyzed by ESR (Fig. 6). The spectrum presents the well-known six-peak hyperfine structure corresponding to manganese ions (Mn^{2+}) convoluted by a powder pattern [21]. Though it is possible to make a quantitative analysis of the ESR spectrum, the value found does not help us to estimate the surface density of Mn^{2+} paramagnetic ions. Indeed, this Lavoux limestone is a natural cavity rock where it is not possible to make any hypothesis about the volume repartition of these impurities. However, we will see in Sec. IV that due to the particular shape of the NMRD dispersion curve, the value of σ_s is not necessary to interpret the data. No ferric ions have been detected in this rock.

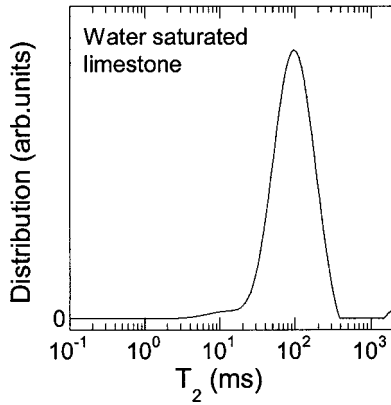


FIG. 5. ^1H spin-spin relaxation time distribution of water saturating a Lavoux limestone at 2.2 MHz and 34 °C. This distribution shows a relatively narrow pore size distribution, allowing an exponential analysis of the magnetization decay.

C. NMR techniques

Proton spin-lattice T_1 and spin-spin T_2 relaxation times were measured at 2.2 MHz on a Resonance Instrument Maran-2 spectrometer England. This low frequency is chosen in the range of a NMR logging tool frequency [15]. T_1 and T_2 were measured using a standard inversion-recovery sequence and a spin-echo CPMG sequence, respectively [20]. Owing to the homogeneity in pore sizes of the samples studied, we used a simple exponential fit to determine the relaxation times. Variation of T_2 with the temperature was measured during the slow decay of the temperature of the cells from 85 to 34 °C [22].

We measured the variations of the spin-lattice relaxation rates with the magnetic field and the temperature using a field cycling instrument of the Redfield design [23] built partly in collaboration with Brown and Koenig of the IBM Watson Laboratory [23,24]. This spectrometer switches the current in a solenoid immersed in liquid nitrogen. Proton spins are first polarized in a magnetic field corresponding to a Larmor frequency of 25 MHz. The magnetic field is then switched to the measured value of interest (corresponding to Larmor frequencies ranging from 0.01 to 25 MHz) for a

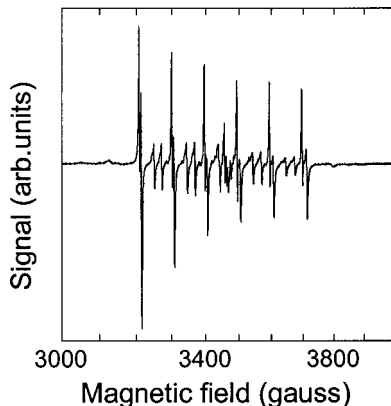


FIG. 6. Electron spin resonance spectrum measured at room temperature on a Lavoux limestone. The six-peak hyperfine structure is typical of Mn^{2+} ions.

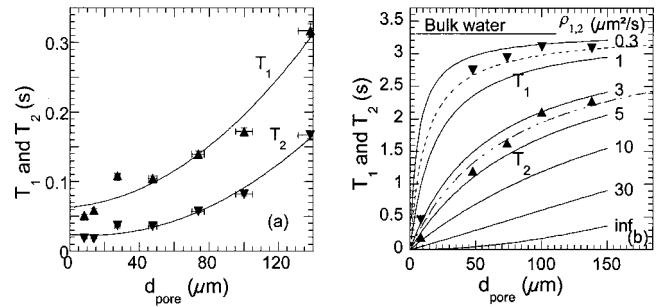


FIG. 7. (a) The ^1H measured water spin-lattice (T_1) and spin-spin (T_2) relaxation times as a function of the pore diameter d_{pore} at 2.2 MHz and 34 °C, before cleaning the surface. The quadratic continuous lines represent the best fits obtained with Eq. 4(a). (b) The measured ^1H water spin-lattice (T_1) and spin-spin (T_2) relaxation times as a function of d_{pore} at 2.2 MHz and 34 °C after cleaning the surface. The continuous lines represent the theoretical pore size dependences calculated with Eq. 4(b), varying the surface relaxivity parameter $\rho_{1,2}$ from 0.3 $\mu\text{m}^2/\text{s}$ to infinity, downwards. The dashed lines represent the best fits obtained with Eqs. 4(b) or 4(c).

variable relaxation period τ after which it is switched to 7.25 MHz, at which the magnetization is detected by a Hahn spin echo. The decay curve is obtained by varying the relaxation period τ and T_1 is determined by the exponential fit of the decay curve. The complete dispersion curve is obtained by repeating this procedure for the different measured field values, ranging from 0.01 and 25 MHz. Measurements were performed at temperatures ranging from 15 to 45 °C, stabilized by a circulation of perchloro-ethylene. Some experiments on water-saturated limestone were repeated on a fast field cycling spectrometer from Stellar Company (Italy).

III. NUCLEAR RELAXATION WITHIN PORES

A. Experiments

Proton nuclear spin-lattice T_1 and spin-spin T_2 relaxation times were measured as a function of the pore size at 2.2 MHz and 34 °C for the water-saturated SiC grain packs described above. The accuracy of the measured T_1 and T_2 are around 3% for fluids in pores and in bulk. One finds a quadratic relationship [Fig. 7(a)] between T_1 or T_2 and the pore size when the surface density of paramagnetic impurities is high (“uncleaned” grain packs). On the contrary, when the surface density of paramagnetic impurities is low (“cleaned” grain packs), one finds another pore size dependence of T_1 or T_2 reaching progressively the asymptotic value $T_{1B} = T_{2B} \approx 0.3$ s of the bulk water [Fig. 7(b)]. Moreover, as expected, the absolute values of the relaxation times for the cleaned and uncleaned samples vary in opposition with the surface density of paramagnetic impurities. The next section provides a theoretical interpretation of the striking observed differences for cleaned and uncleaned samples.

B. Comparison theory—experiments and discussion

Basically, there are two limiting cases in the theoretical description of the relaxation of liquids filling pores with surface relaxation sinks [13,25]. These cases are either

diffusion-limited or surface-limited relaxation, providing that bulk diffusion or surface processes dominate, respectively. Theoretical expressions of the nuclear relaxation rates have been proposed in each limited case [25]. In particular, special interest has been focused on the surface-limited relaxation, corresponding to most of the natural rock data [13,26]. In order to discuss the pore-size data presented in Fig. 7, we describe in Appendix A the general situation when both processes occur. We have considered explicitly the exchange rate W between the surface layer of thickness ε and the bulk, and their respective relaxation times T_{1S} and T_{1B} . One finds at long times t and under the condition of fast exchange, $t \gg T_{1S} \gg 1/W$, an exponential time decay of the longitudinal magnetization with the spin-lattice relaxation rate

$$\frac{1}{T_1} = \frac{1}{T_{1B}} + \frac{1}{\frac{a}{\alpha\rho_1} + \frac{a^2}{2\alpha D}} = \frac{1}{T_{1B}} + \frac{\alpha\rho_1}{a} \frac{1}{1 + \frac{\rho_1 a}{2D}}. \quad (2)$$

In Eq. (2) a is the characteristic dimension of the model pore and $\alpha = 1, 2$, or 3 is the shape factor for planar, cylindrical, and spherical pore geometry, respectively. The efficiency of the surface relaxation is qualified by $\rho_1 = \varepsilon/T_{1S}$ and D is the translational self-diffusion coefficient within the pore. The expression of the spin-spin relaxation is similar, exchanging the indices 1 and 2. Equation (2) shows clearly the independence of bulk and confined relaxation rates, while the confined rate depends on two relaxation processes in series. A direct comparison of $2D/a$ and $\rho_{1,2}$ shows that the slowest process limits the relaxation. For instance, when $\rho_{1,2}a/2D \gg 1$ the relaxation is diffusion limited, and Eq. (2) simplifies

$$\frac{1}{T_{1,2}} = \frac{1}{T_{1,2B}} + \frac{2\alpha D}{a^2}. \quad (3a)$$

On the other hand, when $\rho_{1,2}a/2D \ll 1$, the relaxation is surface limited, and one has

$$\frac{1}{T_{1,2}} = \frac{1}{T_{1,2B}} + \frac{\alpha\rho_{1,2}}{a}. \quad (3b)$$

These expressions thus relate directly the relaxation times T_1 or T_2 to either a^2 or a , providing that the conditions of diffusion-limited or surface-limited relaxation are fulfilled, respectively.

Experimental results show that for the uncleaned porous media presenting a high surface density of paramagnetic impurities [Fig. 7(a)], T_1 and T_2 relaxation times of water vary as the square of the pore diameter $d_{\text{pore}} = 2a$ (quasispherical pores). This dependence agrees with the diffusion-limited relaxation [Eq. 3(a)], which becomes

$$\frac{1}{T_{1,2}} = \frac{1}{T_{1,2B}} + \frac{24D}{d_{\text{pore}}^2} \approx \frac{24D}{d_{\text{pore}}^2}. \quad (4a)$$

In Eq. (4a) the measured bulk water relaxation rates, $1/T_{1B} = 1/T_{2B} \sim 0.3 \text{ s}^{-1}$, can be neglected. Such a relation thus provides an estimation of the translational diffusion coefficient in pores $D = 2.3 \times 10^{-5} \text{ cm}^2/\text{s}$ at 34°C from the T_1 data.

This value is slightly lower than the bulk value $D = 3 \times 10^{-5} \text{ cm}^2/\text{s}$ expected at this temperature. This slight difference is due to the confinement of the fluid and gives us confidence about the validity of the proposed model. We obtain $D = 4.7 \times 10^{-5} \text{ cm}^2/\text{s}$ from the T_2 data, which is higher than the first estimation. In this uncleaned material, this difference may be due to the presence of non-negligible internal field gradients, coming from the contrast of susceptibility between fluid and grain parts of the pore, which affects the CPMG measurements [27,28]. We note that all the grains were obtained by the same grinding process applied to the same SiC material. Therefore, we expect that the surface density of paramagnetic impurities before cleaning does not vary very much from one grain size to the other. We have performed some ESR measurements, which are very noisy and difficult to interpret. However, the Fig. 3 proves the presence of a large amount of surface impurities, before cleaning, which could create some complex electronic spin states. However, the exact knowledge of the surface density of paramagnetic ions is not needed as soon as the condition of diffusion-limited regime ($\rho d_{\text{pore}}/4D \gg 1$) is reached [see Fig. 7(a)]. In the rest of the paper we were only concerned with cleaned samples in the surface-limited regime, which is of considerable interest as this regime is encountered in the majority of natural rocks.

Experimental results show another pore size dependence of T_1 and T_2 for the cleaned porous media that reaches asymptotically the bulk relaxation time [Fig. 7(b)]. The uncertainty resulting from the small difference between the relaxation times of the largest pores and the bulk value requires a more conservative and general approach than the immediate use of Eq. (3b).

We first note that we have obtained the same surface density of paramagnetic ferric impurities for all the samples of various grain sizes by ESR experiments and interpretations described in Sec. II A. So it is meaningful to study the pore size dependence of the nuclear-spin relaxation rates of water within this set of cleaned samples.

The general situation that describes the nuclear-spin relaxation of a liquid in confinement is presented in Appendix A, where both surface-limited and diffusion-limited processes occur in series. This leads to the spin relaxation rate given for a spherical pore by

$$\frac{1}{T_{1,2}} = \frac{1}{T_{1,2B}} + \frac{1}{\frac{d_{\text{pore}}}{6\rho_{1,2}} + \frac{d_{\text{pore}}^2}{24D}} = \frac{1}{T_{1,2B}} + \frac{6\rho_{1,2}}{d_{\text{pore}}} \frac{1}{1 + \frac{\rho_{1,2}d_{\text{pore}}}{4D}}. \quad (4b)$$

The experimental results for T_1 and T_2 are displayed in Fig. 7(b) in comparison with a set of theoretical pore size dependences calculated with Eq. (4b) varying the surface relaxivity parameters $\rho_{1,2}$ ($\mu\text{m/s}$) from a very small value to infinity. In Eq. (4b) we used $1/T_{1,2B} \sim 0.3 \text{ s}^{-1}$ and the measured diffusion coefficient $D = 2.3 \times 10^{-5} \text{ cm}^2/\text{s}$ of water in pores. These theoretical dependences thus cover the complete range between the pure surface-limited relaxation process, when $\rho_{1,2}d_{\text{pore}}/4D \ll 1$, described by

$$\frac{1}{T_{1,2}} = \frac{1}{T_{1,2B}} + \frac{6\rho_{1,2}}{d_{\text{pore}}} \quad (4c)$$

and the pure diffusion-limited relaxation process, when $\rho_{1,2}d_{\text{pore}}/4D \gg 1$, described by Eq. (4a). The change of behavior of these theoretical pore size dependences in the two extreme parts of the range of surface relaxivity parameters $\rho_{1,2}$ gives a clear information about the leading limiting relaxation regime. The location of the experimental points in Fig. 7(b), compared with the theoretical behavior, reveals an intrinsic coherence in our experiments, allowing us to enclose our data in a range of surface relaxivity parameters. For instance, we propose the following ranges: $0.3 \leq \rho_1 \leq 1 \mu\text{m/s}$ and $3 \leq \rho_2 \leq 5 \mu\text{m/s}$, with an average value determined by the best fits, $\rho_1 = 0.6 \mu\text{m/s}$ and $\rho_2 = 3.7 \mu\text{m/s}$, obtained with Eq. (4b) and represented by the dashed lines in Fig. 7(b). The calculations made for $\rho_{1,2}d_{\text{pore}}/4D$ with these two latter values of $\rho_{1,2}$, even in the worst case of $d_{\text{pore}} = 138 \mu\text{m}$, give the estimations $\rho_1 d_{\text{pore}}/4D = 9 \times 10^{-3}$ and $\rho_2 d_{\text{pore}}/4D = 0.056$. The conditions $\rho_{1,2}d_{\text{pore}}/4D \ll 1$ show that the pore size dependences of these cleaned samples are finally better described by the surface-limited relaxation process rather than by the diffusion-limited relaxation process. Moreover, the use of Eq. (4c), corresponding to the surface-limited relaxation regime, gives the same average values of ρ_1 and ρ_2 .

Last, we have measured the internal gradients for all the water-saturated grain packs, from the variation of the measured $1/T_2$ relaxation rates of the CPMG sequence with the interecho time. We checked that the contribution of the gradient in relaxation rates, $1/T_2$, is negligible for the very short interecho times used [22].

IV. NUCLEAR RELAXATION AT THE PORE SURFACE

It is well known that surface paramagnetic impurities are strong relaxation sinks for the spin-bearing molecules in pores. As seen above, the access to the pore surface is governed by molecular diffusion and biphasic fast exchange between the surface layer and the bulk. Now, we aim to characterize the dynamical processes at the origin of the surface relaxivity ρ_1 of liquids, occurring at the pore surface. These processes depend mainly on the nature of the liquid and its affinity for the pore surface. For instance, the possibility of exchanging protons is determinant in the liquid dynamics at the solid-liquid interface. This will also enhance the value of the relaxation rates, especially in the presence of surface paramagnetic impurities. However, probing directly the surface dynamics of proton species in saturated large pores is difficult due to the very low ratio of the surface to bulk amount of molecules. Two conditions will favor the surface study. (i) The biphasic fast exchange condition allows every molecule in the pore to probe temporarily the surface. (ii) The use of the field cycling technique enhances the dynamical range of information covering all the possible surface events. We present below the nuclear magnetic relaxation dispersion data (NMRD) of spin-lattice relaxation rates $1/T_1$ of water- or oil-(dodecane) saturated $8 \mu\text{m}$ grain packs and limestone cores and their interpretations in terms of an

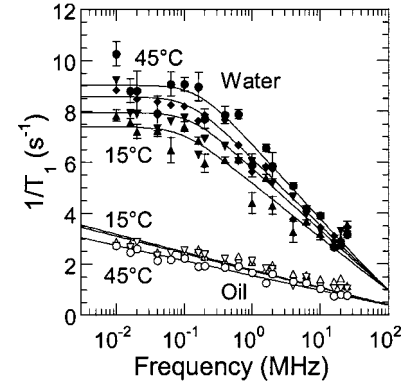


FIG. 8. Measured water and oil (dodecane) ^1H spin-lattice relaxation rates, saturating the $8 \mu\text{m}$ grain pack after cleaning the surface, as a function of the proton Larmor frequency, for different temperatures: 45°C (\bullet), 35°C (\blacklozenge), 25°C (\blacktriangledown), and 15°C (\blacktriangle) for water and 15°C (\triangle), 25°C (\triangledown), and 45°C (\circ) for oil. The continuous lines correspond to the fits obtained with Eq. (9).

original theoretical model to follow the frequency (ω) and temperature (T) dependence of $\rho_1(\omega, T)$.

A. Field cycling experiments

1. $8 \mu\text{m}$ grain packs

The cleaned $8 \mu\text{m}$ SiC grain packs were specially prepared for the field cycling spectrometer in cells of 0.8 cm in diameter and 1.5 cm in length and filled with water or oil, the extra liquid on top being removed. The magnetic field variations of the measured longitudinal relaxation rates, $1/T_1$, for both water and oil saturation, are displayed in Fig. 8. The measurements are reported for magnetic fields corresponding to Larmor frequencies ranging between 0.01 and 25 MHz from 15 to 45°C .

Inspection of Fig. 8 leads to the following immediate conclusions. (i) Water relaxation rates are higher than oil ones. These differences are due to the different distances of minimal approach of these polar and nonpolar liquids near the relaxing sources, namely the paramagnetic impurities, thus revealing the expected difference in the affinity of these two liquids for the pore surface. However, we mentioned that 25% of the surface is covered by SiO_2 and 75% by SiC. This SiC surface is less hydrophilic than the SiO_2 surface, so that it is more likely that dodecane molecules reach directly this part of the surface of the grains. (ii) The frequency dependence is different for water and oil. Water dispersion curves vary logarithmically with the magnetic field, and terminate by a plateau below a specific cutoff value at low field. Oil dispersion curves vary logarithmically with the magnetic field in the whole field range studied, but with a much smaller slope. (iii) The temperature dependence of the relaxation rates $1/T_1$ has the opposite sign for water and oil. This is specifically important as it shows the role of the water proton exchange with the surface protons [11], while for the dodecane molecule the protons are nonexchangeable.

To emphasize water and oil differences, we report on two Arrhenius plots, the temperature dependence of $1/T_1$ for various Larmor frequencies for water [Fig. 9(a)] and oil [Fig.

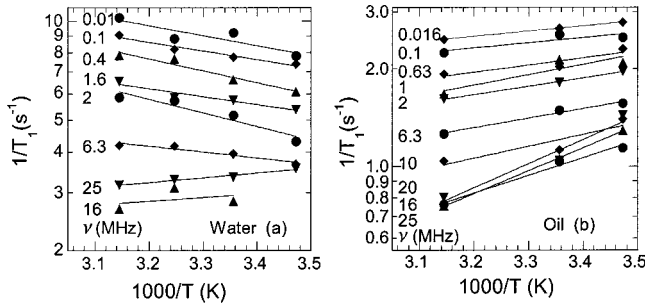


FIG. 9. Arrhenius diagrams of the measured ^1H relaxation rates, saturating the $8\ \mu\text{m}$ grain size pack after cleaning the surface, as a function of the inverse of temperature for different proton Larmor frequencies (a) for water and (b) for oil.

9(b)], respectively. Usually, $1/T_1$ increases exponentially with the inverse of the temperature revealing activated rotational or translational molecular diffusive motions. This is observed for oil at all frequencies, and for water at frequencies above 10 MHz [Figs. 9(a) and 9(b)]. On the contrary, below 10 MHz, the water temperature dependence is inverted [Fig. 9(a)]. Such anomalous temperature dependence has been observed previously in nanopores and has required an interpretation in terms of a specific surface diffusion process [11].

2. Limestone

The NMRD curves of $1/T_1$ for both water or oil saturation in core limestone are reported in Fig. 10 for frequencies ranging between 0.01 and 25 MHz from 15 to 45 °C. Inspection of Fig. 10 leads to the following immediate conclusions. (i) As previously observed, relaxation rates are higher for water than for oil. This is consistent with the expected higher surface affinity of water compared to dodecane. This is also consistent with the shorter distances of minimal approach near the relaxing sources for water than for dodecane. A monolayer of water might cover the surface and enhance this minimal distance, even in the presence of dodecane satura-

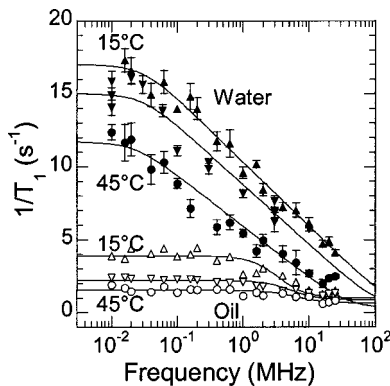


FIG. 10. Measured water and oil (dodecane) ^1H spin-lattice relaxation rates, saturating the limestone rock, as a function of the proton Larmor frequency for different temperatures: 15 °C (\blacktriangle), 23 °C (\blacktriangledown), and 45 °C (\bullet) for water and 15 °C (\triangle), 25 °C (\triangledown), and 45 °C (\circ) for oil. The continuous lines correspond to the fits obtained with Eq. (11).

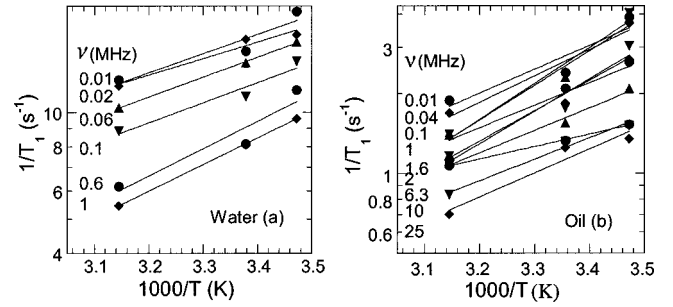


FIG. 11. Arrhenius diagrams of the measured ^1H relaxation rates, saturating the limestone rock, as a function of the inverse of temperature for different proton Larmor frequencies (a) for water and (b) for oil.

tion. This last monolayer of water at the pore surface is extremely difficult to remove in such samples. (ii) Water dispersion curves vary logarithmically with the frequency, and terminate by a plateau below a very low frequency cutoff. Oil dispersion curves follow Lorentzian-like frequency dependence. (iii) The spin-lattice relaxation rates for both water and oil present a normal temperature dependence for the different Larmor frequencies [Figs. 11(a) and 11(b)]. This dependence reveals activated rotational or translational molecular diffusive motions. To interpret completely these different observed frequency and temperature variations of the relaxation rates, an original theoretical model is required.

B. Calculation of NMRD of surface spin-lattice relaxation rate

We consider an ensemble of proton spin-bearing molecules ($I = \frac{1}{2}$) diffusing within a porous media with a given surface density σ_S of paramagnetic impurities of electronic spin S ($S = \frac{5}{2}$ for Fe^{3+} and Mn^{2+}). Basically, we consider two phases: a surface-affected liquid phase of spin-lattice relaxation rate $1/T_{1S}$ and a bulk liquid phase of spin-lattice relaxation rate $1/T_{1B}$, and we suppose that the exchange rate W between them is much larger than both relaxation rates $1/T_{1S}$ and $1/T_{1B}$. According to this biphasic fast exchange model, and generalizing Eq. (4c) (surface-limited relaxation process) to a porous system of surface to volume ratio S_p/V_p , the overall proton spin-lattice relaxation rate, $1/T_1(\omega_I, T)$, is

$$\frac{1}{T_1(\omega_I, T)} = \frac{1}{T_{1B}} + \rho_1(\omega_I, T) \frac{S_p}{V_p} = \frac{1}{T_{1B}} + \frac{N_S}{N} \frac{1}{T_{1S}(\omega_I, T)}. \quad (5)$$

In Eq. (5), the bulk contribution appears to be frequency independent at low magnetic fields due to its Lorentzian behavior. On the contrary all the frequency dependence comes from the surface contribution, where N_S/N represents the ratio of the pore surface to the total amount of water molecules. Due to the paramagnetic impurities, the dominant contribution of the proton (I) nuclear relaxation $1/T_{1S}(\omega_I, T)$ comes from the heteronuclear dipole-dipole interaction with the electronic spins (S), formally given by [20]

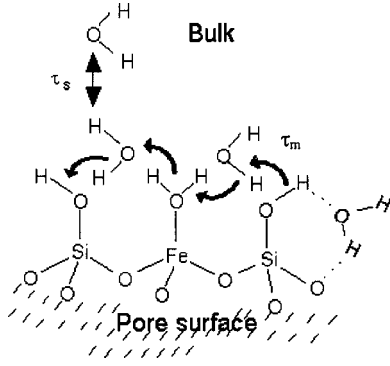


FIG. 12. Schematic diagram of surface diffusion of the proton species of water on a silica surface limited by exchange with bulk water.

$$\frac{1}{T_{1S}} = \frac{2}{3} (\gamma_I \gamma_S \hbar)^2 S(S+1) \left[\frac{1}{3} J_L^{(0)}(\omega_I - \omega_S) + J_L^{(1)}(\omega_I) + 2J_L^{(2)}(\omega_I + \omega_S) \right], \quad (6)$$

where the Larmor frequencies of the electron and proton are related by $\omega_S = 658.21\omega_I$. The spectral densities $J_L^{(m)}(\omega)$ ($m=0, \pm 1, \pm 2$), in the laboratory frame (L) associated with the constant magnetic field \mathbf{B}_0 are the exponential Fourier transform of the pairwise dipolar correlation functions $G_L^{(m)}(\tau)$:

$$J_L^{(m)}(\omega) = \int_{-\infty}^{+\infty} G_L^{(m)}(\tau) e^{-i\omega\tau} d\tau. \quad (7)$$

The basic principles of nuclear paramagnetic relaxation show that the proton nuclear relaxation is controlled by two different correlation times both dependent on liquid motion and electron spin relaxation [29]. The difference between these two correlation times comes from the electron longitudinal or transverse spin relaxation contributions. The relative importance of these two latter times and the relation $\omega_S = 658.21\omega_I$ allows us to simplify Eq. (6),

$$\frac{1}{T_{1S}} = \frac{2}{3} (\gamma_I \gamma_S \hbar)^2 S(S+1) J_L^{(1)}(\omega_I). \quad (8)$$

Here we have extended the theory by focusing on the frequency dependence of the surface spin-lattice relaxation rate $1/T_{1S}(\omega_I, T)$. To calculate the spectral density $J_L^{(1)}(\omega_I)$, we consider a surface diffusive model where the dipole-dipole (I - S) interaction is modulated by the two-dimensional translational diffusion of the mobile spin I in the dipolar field of the electronic spin S fixed at the pore surface. The correlation time of surface diffusion events is characterized by τ_m . We also incorporate in the model the molecular surface desorption in terms of finite residence time τ_s of the protons moving on the pore surface (Fig. 12). Such a consideration is of particular importance to explain the differences of surface affinity of water and oil in porous media. We outlined the calculation of $J_L^{(1)}(\omega)$ in Appendix B. Successive substitu-

tions of Eq. (B2) into Eqs. (8) and (5) lead to the general expression of the proton spin-lattice relaxation rates in pores,

$$\frac{1}{T_1(\omega_I, T)} = \frac{1}{T_{1B}} + \frac{N_S}{N} \frac{\pi}{20} \frac{\sigma_S}{\delta^4} (\gamma_I \gamma_S \hbar)^2 S(S+1) \times \tau_m(T) \ln \left[\frac{1 + \omega_I^2 \tau_m^2(T)}{\left(\frac{\tau_m(T)}{\tau_S(T)} \right)^2 + \omega_I^2 \tau_m^2(T)} \right]. \quad (9)$$

This expression gives a logarithmic nuclear magnetic relaxation dispersion (NMRD) with a leveling off below a frequency cutoff ω_{Ico} . Such a behavior corresponds quite well to our observation for water-saturated grain packs (Fig. 8). The typical dispersion curves obtained thus allow us to access directly to the two surface correlation times τ_m and τ_s of the model. For instance, τ_s is given by $\tau_s = 1/\omega_{Ico}$ and τ_m is estimated from the slope of the logarithmic NMRD data. We introduce the notion of surface ‘‘affinity’’ given by the ratio τ_s/τ_m , which corresponds to the number of molecular diffusing steps precisely on the solid surface, before ‘‘desorption.’’ There exists some recent and very sophisticated high-resolution two-dimensional NMR technique, which could measure the time of residence of water at the surface of a macromolecule. But this latter method is meaningless for a solid surface. The knowledge of an isotherm of adsorption of water might give complementary information on the liquid-solid interaction. Now it could be also useful to relate our local affinity measurement to some macroscopic wettability measurement through capillary pressure curves [16].

The temperature dependence of $1/T_1(\omega_I, T)$ appears via the activated laws of correlation times τ_m and τ_s ,

$$\tau_m(T) = \tau_{m0} \exp\left(\frac{\Delta E}{R_b T}\right), \quad (10a)$$

$$\tau_s(T) = \tau_{s0} \exp\left(\frac{E_S}{R_b T}\right). \quad (10b)$$

Here R_b is the gas constant, ΔE is an apparent activation energy expressed as a difference $\Delta E = E_m - E_S$ of the activation energy for liquid translational diffusion E_m and the energy E_S of the potential binding between the probed molecules and the surface. E_S depends on the type of interaction with the surface. For instance, for silica surface its value is larger than E_m , leading to a negative ΔE , and to a surface correlation time τ_m for diffusion events apparently increasing with the temperature T . This effect corresponds to the surface diffusion induced by the chemical exchange in the surface layer. This effect is limited by another exchange with the bulk population, schematically described in Fig. 12.

The main interest in using the field cycling NMRD technique for probing $1/T_1(\omega_I, T)$ is to separate surface and bulk liquid dynamics. The surface dynamics is responsible for the important logarithmic dispersion seen at low frequency, while the bulk dynamics gives only a small and frequency invariant contribution, which can be neglected in this range of frequency. The direct comparison of Eqs. (9) and (5)

shows that the frequency and temperature variation of the surface relaxivity $\rho_1(\omega_I, T)$ is directly proportional to that of the measured relaxation rate $1/T_1(\omega_I, T)$. The coefficient of proportionality is the volume to surface ratio V_p/S_p of the pores that could be measured with the pulsed field gradient method [30,31].

C. Comparison theory—experiments and discussion

1. 8 μm grain packs

The experimental dispersion curves of $1/T_1(\omega_I, T)$, displayed in Fig. 8, present a logarithmic behavior with a leveling off for water below the frequency cutoff ω_{Ico} , in agreement with Eq. (9). This logarithmic behavior is the unambiguous signature of the two-dimensional proton species diffusion in the surface layer [32]. The loss of frequency dependence for $\omega_I < \omega_{Ico}$ is due to the absence of dipolar correlations between I and S spins after molecular surface desorption. As described above, these typical dispersion curves allow us to access directly to the two surface correlation times τ_m and τ_S of the model. One notices that there is more than a factor 2 between the relaxation time measured at 2 MHz by the field cycling method and by the standard method described in Sec. III. A possible explanation comes from the fact that the response time of the field cycling measurement may bias the measurement. Any fast decay is then usually missed because of the necessary finite field switching time. Another explanation might originate from the fact that the same lot of cleaned calibrated grains of 8 μm was used in series for the two experiments after successive drying and resaturation. This method does not prevent us from partial oxidation of the sample surface.

The best fits obtained with Eq. (9) for the cleaned 8 μm grain packs NMRD of $1/T_1(\omega_I, T)$ are shown as continuous lines in Fig. 8. Let us consider first the results of water. Almost all parameters present in Eq. (9) are either known or measured independently. The only adjustable parameter is the surface translational diffusion correlation time τ_m . The paramagnetic surface density $\sigma_S = 1.7 \times 10^{13} \text{ Fe}^{3+}/\text{cm}^2$ is obtained by ESR measurements ($S = \frac{5}{2}$). The ratio between surface and total amounts of water molecules is modeled as $N_S/N = 6\varepsilon/d_{\text{pore}}$, where the surface layer width $\varepsilon = 3.8 \text{ \AA}$ is chosen as the order of the water molecular size. The distance of minimal approach δ between I and S spins is chosen as ε . The time of surface residence is related to the observed frequency cutoff $\omega_{Ico} \sim 0.1 \times 2\pi \times 10^6 \text{ rad/s}$ as $\tau_S \sim 1/\omega_{Ico} = 1.6 \mu\text{s}$ (at 25 °C). The correlation time of surface diffusion is found as $\tau_m \approx 0.6 \text{ ns}$ at 25 °C. The effective surface diffusion coefficient of the water proton species on the silica surface is thus estimated as $D_{\text{eff}} \sim \varepsilon^2/(4\tau_m) = 6 \times 10^{-7} \text{ cm}^2/\text{s}$, which is much smaller than the bulk water. A similar value has been measured by the pulsed field gradient spin-echo NMR at the surface of silica for a surface monolayer [1]. Owing to the water-surface interaction, it makes sense that the surface diffusion coefficient is reduced. This might be due to the relatively high surface density of ferric ion and to the value of the enthalpy of metal-ion-water dissociation, $\Delta H = 7.4 \text{ kcal/mol}$, for the exchange of water from the ferric cation [33] which hinders the surface diffusion. From the two

surface correlation times, a coefficient of surface molecular affinity is defined as the ratio $\tau_S/\tau_m \sim 2700$, giving the number of molecular jumps during the surface residence time. We note that τ_m can be directly obtained without the knowledge of all the constant parameters of Eq. (9). Considering the frequency cutoff, the slope of the logarithmic variation and the value of the relaxation rate of the plateau $1/T_{1\text{plateau}}$ for $\omega_I \gg \omega_{Ico}$, the relaxation rates vary in frequency as

$$\frac{1}{T_1} = \frac{1}{2T_{1\text{plateau}}} \ln \left(1 + \frac{1}{(\omega_I \tau_m)^2} \right) \bigg/ \ln [1/(\omega_{Ico} \tau_m)]. \quad (11)$$

This very simple method confirms the results found above. One of the interesting points of Eq. (11) is that the values of S_p/V_p and σ_S are not needed to fit the dispersion curves, as soon as we know the value of the plateau and of the slope of the logarithmic part of the curve. However, Eq. (11) can be applied only in presence of a plateau in the NMRD data.

Another striking result is the temperature dependence of $1/T_1$ observed for water [Fig. 9(a)]. In the high frequency range, the observed usual temperature dependence is coherent with an activated fast translational diffusion of bulk water characterized by the activation energy $E_m = 4.8 \text{ kcal/mol}$. In the low frequency range, the observed anomalous temperature behavior allows us to find an apparent activation energy $\Delta E = E_m - E_S = -2 \text{ kcal/mol}$ for the water proton mobility in the surface layer. From these values of E_m and ΔE , we deduce the activation energy $E_S = 6.8 \text{ kcal/mol}$ that might correspond to a particular surface interaction [11]. The effective diffusion of the proton species is modeled at the pore surface in the schematic diagram of Fig. 12. Such a diffusion occurs through a succession of exchange processes within the first layer of water molecules and is limited by another exchange with the bulk. The population of such layered water molecules varies as a Boltzmann factor $[\exp(E_S/R_b T)]$ that decreases when the temperature increases. On the contrary, the usual diffusion coefficient increases with T as $D_m(T) = D_{m0} \exp(-E_m/R_b T)$. In consequence, to interpret our data, we consider an effective surface diffusion coefficient $D_{\text{eff}}(T) = D_{\text{eff}0} \exp[(E_S - E_m)/R_b T] = D_{\text{eff}0} \exp[-\Delta E/R_b T]$, which apparently decreases when T increases because $\Delta E < 0$.

For the dodecane molecule, the NMRD present a weak logarithmic dependence with the magnetic field with no leveling off (Fig. 8) and a pure diffusive temperature behavior [Fig. 9(b)]. This frequency dependence is rather surprising for such a large flexible molecule. We expected an intramolecular (I-I) dipolar relaxation process by molecular reorientation in a quasispherical molecule leading to a Lorentzian NMRD. On the contrary, the logarithmic dependence proves that this molecule presents an asymmetric conformation, which does not average out the internal proton dipolar correlation at proximity of the surface. The dominant relaxation process for oil thus comes from the translational motion at proximity of the paramagnetic species. From the fit of our data, we estimate the diffusion correlation time $\tau_m \sim 0.4 \text{ ns}$, and the effective surface diffusion $D_{\text{eff}} \sim \varepsilon^2/(4\tau_m) \sim 1.5 \times 10^{-6} \text{ cm}^2/\text{s}$. Due to the absence of exchange of the

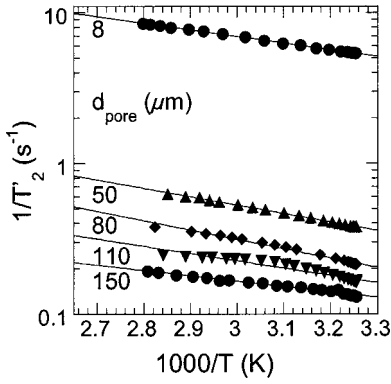


FIG. 13. Water ^1H spin-spin relaxation rates as a function of the inverse of temperature for the different pore sizes, after cleaning the surface, at 2.2 MHz, and after correction of the bulk contribution.

protons with the surface, we choose $\Delta E = E_m$, in accordance with the normal temperature dependence observed for $1/T_1$ [Fig. 9(b)].

2. Temperature dependence of the spin-spin nuclear relaxation rates

In complement, we measured the temperature dependence of the proton spin-spin relaxation rates $1/T_2$ of the water-saturated cleaned grain packs for every pore size (ranging from 8 to 150 μm). After the correction of the bulk contribution, one obtains the rates $1/T_2'$ presented in Arrhenius plots on Fig. 13. The data series of each pore size are fitted by exponential curves. The results obtained confirm the observed anomalous temperature effect seen for $1/T_1$. In particular, we find the same activation energy $\Delta E = E_m - E_S$, ranging from -2 to -2.8 kcal/mol as found for $1/T_1$. More generally, these results prove the anomalous temperature dependence of ρ_2 of silica surfaces. We recently found the same temperature dependence on water-saturated Fontainebleau sandstone.

3. Limestone cores

The experimental water dispersion curves of $1/T_1(\omega_I, T)$ present a logarithmic frequency dependence characteristic of a two-dimensional surface diffusion (Fig. 10). A plateau appears below a very low frequency cutoff, revealing a longer value of the surface residence time τ_S than for a silica surface. Moreover, the temperature dependence of $1/T_1$ [Fig. 11(a)] is typical of a pure diffusive process. Due to the difficulty of estimating the density of paramagnetic impurities at the surface, we directly used the simplified Eq. (11) to extract the surface correlation times from the NMRD data. The best fits are shown as continuous lines in Fig. 10. The time of surface residence is related to the observed frequency cutoff $\omega_{Ico} \sim 0.03 \times 2\pi \times 10^6$ rad/s as $\tau_S \sim 1/\omega_{Ico} = 5.3 \mu\text{s}$ (at 25 $^\circ\text{C}$). We find a correlation time $\tau_m = 1.3$ ns at 23 $^\circ\text{C}$, leading to a surface diffusion coefficient $D_{\text{eff}} = 2.5 \times 10^{-7}$ cm^2/s , which is two orders of magnitude slower than for the bulk. This slow two-dimensional diffusion might be interpreted as the diffusion of hydrated calcium anions instead of water molecules at proximity of the very reactive

CaCO_3 surface. The coefficient of surface molecular affinity, $\tau_S/\tau_m \sim 4100$, giving the number of molecular jumps during the surface residence time, is higher than the coefficient of silica surface. One notices a slight difference (40%) between the T_1 values measured at 2.2 MHz by the standard method and by the field cycling method. As previously mentioned for the measurements in grain packings, the problem might arise from the response time of the field switch, which may bias the measurement. This might also be due to the size of the core used for the field cycling method. The small core might not integrate the total complexity of pore size of the natural rock as the large core used for the standard measurement.

We recently performed other experiments on similar materials at other temperatures that reveal a transition to a bilogarithmic character of the NMRD curves, typical of a bidimensional two-frequency (electronic and nuclear) problem [10]. Such a bilogarithmic character can be easily obtained with the theory proposed in Sec. IV B by considering the spectral densities [Eq. (B2)] at electronic and nuclear frequencies Eq. (6) with $\omega_S \gg \omega_I$. However, all the surface dynamical parameters are of the same order of magnitude than the one described above.

The situation for the dodecane dispersion data is very different than for the water one. The leveling off occurs at a much higher cutoff frequency $\omega_{Ico} \sim 1 \times 2\pi \times 10^6$ rad/s. The dispersion curves, displayed in Fig. 10, are almost Lorentzian-like. The temperature behavior is typical of a pure diffusive process [Fig. 11(b)]. The best fits obtained with Eq. (11) indicate that the time of residence on the surface ($\tau_S \sim 20\tau_m$) is not sufficiently long to induce a logarithmic frequency behavior. We check that the limiting expression of Eq. (9) when $\omega_I\tau_m \ll 1$ and $\tau_S/\tau_m \gg 1$ behaves in frequency like a Lorentzian. Such dispersion data thus reveals a much lower affinity of dodecane for the limestone surface than for the silica surface. In consequence, the reorientation of a quasispherical conformation of the dodecane molecule at proximity of the paramagnetic species (Mn^{2+}) is probably the dominant relaxation process.

V. CONCLUSION

On the basis of experimental and theoretical nuclear relaxation results obtained at various conditions of temperature, magnetic field strengths, and pore size, we find surface dynamical parameters from the relaxation rates $1/T_1$ and $1/T_2$ of water and oil liquids confined in calibrated grain packs and limestone rocks. Both porous media are homogeneous in pore sizes and present some paramagnetic impurities (Fe^{3+} or Mn^{2+}) that have been analyzed by electron spin resonance (ESR). We observed striking different pore size dependences of the relaxation times T_1 and T_2 at 2.2 MHz by changing the surface amount of paramagnetic impurities. These observations support a theoretical model of pore size dependence of relaxation rates in terms of surface-limited or diffusion-limited relaxation processes. For the surface-limited processes, we evaluated the surface relaxivity parameters ρ_1 and ρ_2 directly from the pore size dependence of T_1 and T_2 , respectively. These parameters, of the order of that estimated in natural rocks, justify the surface-limited relax-

ation process as relevant in natural rocks. We evidenced the variation of the surface relaxivity $\rho_1(\omega_f, T)$ with the frequency and the temperature by the nuclear magnetic relaxation dispersion technique (field cycling NMRD). This technique and the theoretical model that we propose allow evidencing properly the surface liquid microdynamics in fully saturated porous media. For instance, we showed that water molecules on a silica surface follow a two-dimensional surface diffusive motion, before desorption from the pore surface. Several surface dynamical parameters, such as diffusion coefficients, activation energies, surface residence time, and the coefficient of surface affinity, were therefore determined. The methods presented here give a powerful analysis of the surface microdynamics of confined liquids, which can be applicable to the study of oil-bearing rocks.

ACKNOWLEDGMENTS

The authors gratefully acknowledge stimulating discussions with Dr. C. Chachaty (Saclay), Dr. D. Petit, Dr. P. Levitz, Dr. F. Beuneu (École Polytechnique), and Dr. G. Chauveteau (IFP).

APPENDIX A: SPIN-RELAXATION IN CONFINEMENT

We consider a liquid saturating a spherical pore of radius a . We enlarge the description for other pore geometry at the end of the appendix. The thickness ε of the liquid surface layer is assumed much smaller than a . Through the presence of paramagnetic impurities, the surface of the pore acts as a relaxation sink for the liquid. We introduce the longitudinal bulk $m_B(r, t)$ and surface $\varepsilon m_S(t)$ magnetization densities in this spherical geometry at a given position r and time t . We consider the new variables $M_B(r, t) = m_B(r, t) - m_{\text{eq}}$ and $M_S(t) = m_S(t) - m_{\text{eq}}$ where m_{eq} is the longitudinal equilibrium magnetization density. The longitudinal magnetization densities obey the generalized and coupled Bloch equations:

$$\varepsilon \frac{dM_S(t)}{dt} = -\frac{\varepsilon}{T_{1S}} M_S(t) - W\varepsilon [M_S(t) - M_B(r=a, t)], \quad (\text{A1a})$$

$$\frac{\partial M_B(r, t)}{\partial t} = -\frac{1}{T_{1B}} M_B(r, t) + D\nabla^2 M_B(r, t), \quad (\text{A1b})$$

where T_{1B} and T_{1S} are the bulk and surface longitudinal relaxation times, respectively, D is the translational diffusion coefficient of the liquid, and W describes the rate of exchange between the surface and bulk magnetization at the surface layer. This rate W might be either a chemical exchange between two different proton species or, more generally, a physical exchange between surface and bulk liquids. The first equation describes the variation of the surface magnetization by nuclear relaxation with the surface paramagnetic impurities and exchange with the bulk magnetization close to the surface. The second equation describes the two possibilities of modifying the bulk magnetization by nuclear relaxation and translational diffusion within the pore. Initially, one has a uniform bulk magnetization density

$$M_B(r, 0) = M_B(0). \quad (\text{A2})$$

The boundary condition at the surface ($r \sim a$) describes the equivalence between normal magnetization flux and magnetization loss by exchange:

$$D \left. \frac{\partial M_B(r, t)}{\partial r} \right|_{r=a} = W\varepsilon [M_S(t) - M_B(a, t)]. \quad (\text{A3})$$

We solve the coupled differential Eqs. (A1) in the Laplace s space, where $\tilde{M}_B(r, s)$ and $\tilde{M}_S(s)$ are the Laplace transforms of bulk and surface magnetizations, respectively. The Laplace transform of Eq. (A3) simplifies at long times, under the condition of fast exchange ($s \ll 1/T_{1S} \ll W$) with the approximation $M_S(0) \ll M_B(0)$,

$$\left. \frac{\partial \tilde{M}_B(\beta r)}{\partial r} \right|_{r=a} = -\frac{\rho_1}{D} \tilde{M}_B(\beta a), \quad (\text{A4})$$

where $\beta = \sqrt{(s + 1/T_{1B})/D}$. Here we take out all the transient effects at short times and qualify the efficiency of the surface relaxation by a constant rate $\rho_1 = \varepsilon/T_{1S}$. Straightforward calculations lead to the solution in the Laplace transform:

$$\tilde{M}_B(\beta r) = \frac{M_B(0)}{D\beta^2} \left[1 - \frac{\rho_1}{D} \frac{\sqrt{\frac{\pi}{2\beta r}} I_{1/2}(\beta r)}{\sqrt{\frac{\pi}{2\beta a} \left(\beta I_{3/2}(\beta a) + \frac{\rho_1}{D} I_{1/2}(\beta a) \right)}} \right], \quad (\text{A5})$$

where $I_{1/2}$ and $I_{3/2}$ are spherical Bessel functions. At long times, $\beta r < \beta a \ll 1$, Eq. (A5) simplifies to a power series which can be integrated over the pore r space, leading to the Laplace transform of the total magnetization $\tilde{M}_{\text{int}}(s)$,

$$\tilde{M}_{\text{int}}(s) = M_B(0) V_p \left[s + \frac{1}{T_{1B}} + \frac{1}{\frac{a}{3\rho_1} + \frac{1}{6D}} \right]^{-1}, \quad (\text{A6})$$

where V_p is the pore volume. Finally a simple Laplace inversion of Eq. (A6) gives an exponential time decay of the magnetization with the following spin-lattice relaxation rate

$$\frac{1}{T_1} = \frac{1}{T_{1B}} + \frac{1}{\frac{a}{3\rho_1} + \frac{1}{6D}}. \quad (\text{A7})$$

A similar treatment for a cylindrical or a pore-slit model, for a longitudinal and transverse relaxation, generalizes Eq. (A7) to the form

$$\frac{1}{T_{1,2}} = \frac{1}{T_{1,2B}} + \frac{1}{\frac{a}{\alpha\rho_{1,2}} + \frac{a^2}{2\alpha D}}, \quad (\text{A8})$$

where $\alpha = 1, 2$, or 3 for planar, cylindrical, and spherical pores, respectively.

APPENDIX B: CALCULATION OF SURFACE DIPOLAR SPECTRAL DENSITY

We have already calculated the spectral density functions in the case of pure two-dimensional diffusive molecular motions [10,11]. In particular, it is much simpler to calculate first the spectral densities $J_M^{(m)}(\omega)$ in the pore surface layer frame M and then to use the well-known properties of the Wigner functions [34,35] for the correspondence between the M and L frames [10]. It is also necessary to make a powder average of $J_M^{(m)}(\omega)$ over all the orientations of the M frame relative to the constant direction of \mathbf{B}_0 [10]. Results of these calculations show that $J_M^{(0)}(\omega)$ dominates largely, at low frequency, over $J_M^{(1)}(\omega)$ and $J_M^{(2)}(\omega)$ and that the only spectral density needed to Eq. (8) simplifies as $J_L^{(1)}(\omega) \sim 1/5 J_M^{(0)}(\omega)$. However, our previous calculations do not consider explicitly the necessary finite surface residence time τ_S due to surface desorption. Here, we incorporate this limiting process in the calculation of $G_M^{(0)}(\tau)$ and then proceed to a simple Fourier transform to obtain $J_M^{(0)}(\omega)$.

From a mathematical point of view, the correlation functions $G_M^{(0)}(\tau)$ must fulfill the three following requirements. (i) At short time, when $\tau \rightarrow 0$, $G_M^{(0)}(\tau)$ must tend to a finite constant A , such as $G_M^{(0)}(0) = \int_{-\infty}^{\infty} J_M^{(0)}(\omega) d\omega = A$ [20]. (ii)

At long time, $G_M^{(0)}(\tau)$ must behave as a power law $1/\tau$ characteristic of a dipolar relaxation process by a two-dimensional translational diffusion [11,32]. Here we simply include the effect of the surface desorption by an exponential cutoff occurring at time τ_S : $G_M^{(0)}(\tau) \propto (A/\tau) \exp(-\tau/\tau_S)$. (iii) We must also consider the form of $G_M^{(0)}(\tau)$ on the time scale of surface molecular diffusion events, $0 \leq \tau \sim \tau_m \ll \tau_S$, characterized by the correlation time τ_m surface diffusion events. Finally, all these requirements lead to the following expression of the correlation function $G_M^{(0)}(\tau)$ which is, as expected, always positive:

$$G_M^{(0)}(\tau) = A \frac{1}{\tau} \left[\exp\left(-\frac{\tau}{\tau_S}\right) - \exp\left(-\frac{\tau}{\tau_m}\right) \right] \Big/ \left(\frac{1}{\tau_m} - \frac{1}{\tau_S} \right) \\ \approx A \frac{\tau_m}{\tau} \left[\exp\left(-\frac{\tau}{\tau_S}\right) - \exp\left(-\frac{\tau}{\tau_m}\right) \right] \quad \text{when } \tau_m \ll \tau_S. \quad (\text{B1})$$

Straightforward calculations similar to those given in the Appendix of Ref. [11] show that $A = 3\pi\sigma_S/8\delta^4$, where σ_S is the surface density of paramagnetic species and δ is the distance of the minimal approach between spins I and S at the pore surface. The spectral density function is thus given by the exponential Fourier transform of Eq. (B1),

$$J_M^{(0)}(\omega) = \frac{3\pi\sigma_S}{8\delta^4} \tau_m \ln \left[\frac{1 + \omega^2 \tau_m^2}{\left(\frac{\tau_m}{\tau_S}\right)^2 + \omega^2 \tau_m^2} \right] \quad (\text{B2})$$

and $J_L^{(1)}(\omega) \sim 1/5 J_M^{(0)}(\omega)$.

-
- [1] F. D'Orazio, S. Bhattacharja, W. P. Halperin, K. Eguchi, and T. Mizusaki, Phys. Rev. B **42**, 9810 (1990).
- [2] J. Y. Jehng, Ph.D. thesis, Northwestern University, 1995.
- [3] G. Liu, Y. Li, and J. Jonas, J. Chem. Phys. **95**, 6892 (1991).
- [4] J.-P. Korb, Shu Xu, and J. Jonas, J. Chem. Phys. **98**, 2411 (1993).
- [5] J.-P. Korb, A. Delville, Shu Xu, G. Demeulenaere, G. Costa, and J. Jonas, J. Chem. Phys. **101**, 7074 (1994).
- [6] J.-P. Korb, L. Malier, F. Cros, Shu Xu, and J. Jonas, Phys. Rev. Lett. **77**, 2312 (1996).
- [7] F. Noack, Bull. Ampere **175**, 18 (1994).
- [8] R. Kimmich and H. W. Weber, Phys. Rev. B **47**, 11 788 (1993).
- [9] M. Whaley, A. J. Lawrence, J.-P. Korb, and R. G. Bryant, Solid State Nucl. Magn. Reson. **7**, 247 (1996).
- [10] J.-P. Korb, M. Whaley-Hodges, and R. G. Bryant, Phys. Rev. E **56**, 1934 (1997).
- [11] J.-P. Korb, M. Whaley-Hodges, Th. Gobron, and R. G. Bryant, Phys. Rev. E **60**, 3097 (1999).
- [12] W. E. Kenyon, Nucl. Geophys. **6**, 153 (1992).
- [13] R. L. Kleinberg, W. E. Kenyon, and P. P. Mitra, J. Magn. Reson., Ser. A **108**, 206 (1994).
- [14] I. Foley, S. A. Farooqui, and R. L. Kleinberg, J. Magn. Reson., Ser. A **123**, 95 (1996).
- [15] R. L. Kleinberg, *Encyclopedia of Nuclear Magnetic Resonance* (Wiley, New York, 1996), Vol. 6, p. 4960.
- [16] R. L. Kleinberg, *Experimental Methods in the Physical Sciences: Methods of the Physics of Porous Media*, edited by P.-Zen Wong.
- [17] V. Médout-Marère, A. El Ghzaoui, C. Charnay, J. M. Douillard, G. Chauveteau, and S. Partyka, J. Colloid Interface Sci. **223**, 205 (2000).
- [18] G. Chauveteau, L. Nabzar, Y. El Attar, and C. Jacquin, in Proceedings of the International Symposium of the Society of Core Analysts, 1996 (unpublished).
- [19] L. Nabzar and G. Chauveteau, SPE 38160, in Proceedings of the European Formation Damage Conference, The Hague, The Netherlands, 1997 (unpublished).
- [20] A. Abragam, *The Principles of Nuclear Magnetism* (Clarendon, Oxford, 1961).
- [21] V. Beltrán-López, Mol. Phys. Rep. **26**, 25 (1999).
- [22] S. Godefroy, J.-P. Korb, D. Petit, and M. Fleury, in Proceedings of the International Symposium of the Society of Core Analysts, Golden, CO, 1999 (unpublished).
- [23] A. G. Redfield, W. Fite, and H. E. Bleich, Rev. Sci. Instrum. **39**, 710 (1968).
- [24] S. H. Koenig and W. E. Schillinger, J. Biol. Chem. **12**, 3283 (1969).

- [25] K. R. Brownstein and C. E. Tarr, *Phys. Rev. A* **19**, 2446 (1979).
- [26] L. L. Latour, R. L. Kleinberg, and A. Sezginer, *J. Colloid Interface Sci.* **150**, 535 (1992).
- [27] D. J. Bergman, K. J. Dunn, and G. A. LaTorraca, *Bull. Am. Phys. Soc.* **40**, 695 (1995).
- [28] M. D. Hurlimann, *J. Magn. Reson.* **131**, 232 (1998).
- [29] J. Korringa, D. O. SeEVERS, and H. C. Torrey, *Phys. Rev.* **127**, 1143 (1962).
- [30] P. P. Mitra, P. N. Sen, L. M. Schwartz, and P. Le Doussal, *Phys. Rev. Lett.* **65**, 3555 (1992).
- [31] P. P. Mitra, P. N. Sen, and L. M. Schwartz, *Phys. Rev. B* **47**, 8565 (1993).
- [32] J.-P. Korb, M. Ahadi, G. P. Zientara, and J. Freed, *J. Chem. Phys.* **86**, 1125 (1987).
- [33] S. K. Sur and R. G. Bryant, *J. Phys. Chem.* **99**, 6301 (1995).
- [34] *Handbook of Mathematical Functions*, edited by M. Abramowitz and I. A. Stegun (Dover, New York, 1972).
- [35] D. A. Varshalovich, A. N. Moskalev, and V. K. Khersonskii, *Quantum Theory of Angular Momentum* (World Scientific, Singapore, 1988).